Journal of Medicinal Chemistry

Article

pubs.acs.org/jmc

Design, Synthesis, and Biological Evaluation of Pyrazolo[3,4-*d*]pyrimidines Active in Vivo on the Bcr-Abl T315I Mutant

Marco Radi,[†,‡] Cristina Tintori,[†] Francesca Musumeci,[§] Chiara Brullo,[§] Claudio Zamperini,[†] Elena Dreassi,[†] Anna Lucia Fallacara,[†,∥] Giulia Vignaroli,[†] Emmanuele Crespan,[⊥] Samantha Zanoli,[⊥] Ilaria Laurenzana,[#] Irene Filippi,[△] Giovanni Maga,[⊥] Silvia Schenone,*[,§] Adriano Angelucci,[○] and Maurizio Botta*[,†,◆]

[†]Dipartimento di Biotecnologie, Chimica e Farmacia, Università degli Studi di Siena, Via Aldo Moro 2, 53100 Siena, Italy

[‡]Dipartimento di Farmacia, Università degli Studi di Parma, Viale delle Scienze 27/A, 43124 Parma, Italy

[§]Dipartimento di Farmacia, Università degli Studi di Genova, Viale Benedetto XV 3, 16132 Genova, Italy

[∥]Dipartimento di Chimica e Tecnologie del Farmaco, Sapienza Università di Roma, Piazzale Aldo Moro 5, 00185 Roma, Italy

[⊥]Istituto di Genetica Molecolare, IGM-CNR, Via Abbiategrasso 207, 27100 Pavia, Italy

[#]Laboratory of Preclinical and Translational Research, IRCCS-Referral Cancer Center of Basilicata (CROB), Rionero in Vulture (PZ), Italy

[△]Dipartimento di Medicina Molecolare e dello Sviluppo, Università degli Studi di Siena, Via Aldo Moro 2, 53100 Siena, Italy

[○]Dipartimento di Scienze Cliniche Applicate e Biotecnologiche, Università dell'Aquila Via Vetoio, 67100 Coppito, L'Aquila, Italy

[◆]Sbarro Institute for Cancer Research and Molecular Medicine, Center for Biotechnology, College of Science and Technology, Temple University, BioLife Science Building, Suite 333, 1900 North 12th Street, Philadelphia, Pennsylvania 19122, United States

Supporting Information

ABSTRACT: Starting from our in-house library of pyrazolo-[3,4-*d*]pyrimidines, a cross-docking simulation was conducted on Bcr-Abl T315I mutant. Among the selected compounds (**2a**–**e**), the 4-bromo derivative **2b** showed the best activity against the Bcr-Abl T315I mutant. Deeper computational studies highlighted the importance of the bromine atom in the para position of the N1 side chain phenyl ring for the interaction with the T315I mutant. A series of 4-bromo derivatives was thus synthesized and biologically evaluated. Compound **2j** showed a good balance of different ADME properties, high activity in cell-free assays, and a submicromolar potency against T315I Bcr-Abl expressing cells. In addition, it was converted into a water-soluble formulation by liposome encapsulation, preserving a good activity on leukemic T315I cells and avoiding the use of DMSO as solubilizing agent. In vivo studies on mice inoculated with 32D-T315I cells and treated with **2j** showed a more than 50% reduction in tumor volumes.

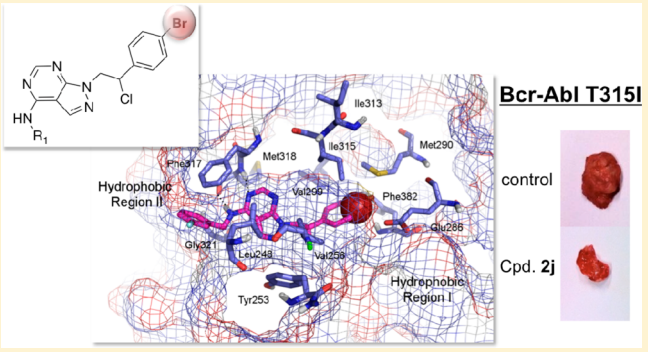

INTRODUCTION

Chronic myeloid leukemia (CML) is a hematological malignancy caused by the constitutively activated kinase Bcr-Abl, resulting from the Philadelphia chromosome (Ph) translocation.[1] Since 2001, the Bcr-Abl tyrosine kinase (TK) inhibitor imatinib (IM) has represented the first line therapy for CML, being particularly active in the chronic phase of the disease, with impressive response and survival rates.[2] However, many patients eventually develop resistance that is frequently associated with mutations in the Bcr-Abl kinase domain.[3] The second-generation Bcr-Abl inhibitor nilotinib[4] and the dual Src/Bcr-Abl inhibitor dasatinib,[5] both approved by FDA for IM-resistant CML treatment, are active against many IM-resistant mutants but proved to be ineffective against the T315I mutation of the gatekeeper residue, which accounts for 15–20% of clinically observed mutations.[6,7]

Preclinical and clinical studies showed that ATP-competitive dual Src/Bcr-Abl inhibitors bosutinib (SKI-606),[8] bafetinib (INNO-406, NS-187),[9] 3-[2-[2-cyclopentyl-6-(4-dimethylphosphorylanilino)purin-9-yl]ethyl]phenol (AP23464),[10] and 6-(2,6-dichlorophenyl)-2-{[3-(hydroxymethyl)phenyl]amino}-8-methylpyrido[2,3-*d*]-pyrimidin-7(8*H*)-one (PD166326)[11] inhibit Bcr-Abl more

Received: February 14, 2013
Published: June 7, 2013

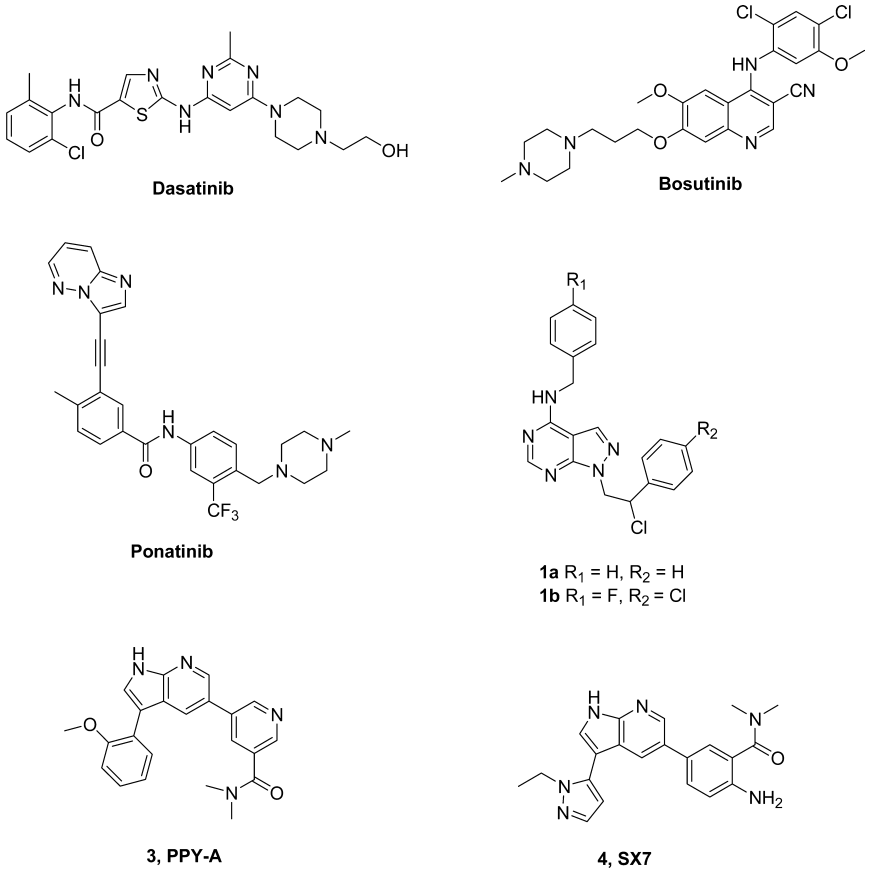

Figure 1. Selected second- and third-generation Bcr-Abl inhibitors.

efficiently than IM and overcome resistance caused by most mutations, with the notable exception of T315I. Optimization of CML treatment remains an area of active research, and much effort has been devoted to the development of more effective TK inhibitors such as ponatinib (AP24534).[12] This compound inhibits both native and mutant Bcr-Abl, including T315I, acting as a pan-Bcr-Abl inhibitor also targeting other TKs.[13]

The T315I point mutation precludes drug binding to the Abl catalytic domain by either direct steric hindrance or stabilization of its active conformation, with the DFG-loop in the "in" disposition (DGF-in).[14] The development of new drugs targeting the open and active conformation of the T315I mutant is therefore a major challenge in CML therapy.[15]

Despite the past efforts to develop selective targeted inhibitors for the treatment of cancer, the main strategy has recently turned to find compounds acting on multiple targets in order to face the drug resistance, often connected with the activation of alternative signaling pathways.[16] Furthermore, Abl shares significant sequence homology and remarkable structural resemblance with Src family members in their active state and several ATP-competitive Src inhibitors targeting the active conformation showed to be also potent Abl inhibitors.[17a] In this context, our research group has deeply investigated a class of pyrazolo[3,4-*d*]pyrimidine derivatives acting as dual inhibitors of Src and Abl kinases. These compounds showed potent antiproliferative and proapoptotic activity toward different cancer cell lines depending on the nature and position of substituents on the heterocyclic core.[18−21]

Recently, we identified two pyrazolo-pyrimidine based Bcr-Abl inhibitors, namely **1a** and **1b** (Figure 1), which were effective against CD34+ cells collected from both imatinib-sensitive and imatinib resistant CML patients, these last bearing the three most frequent Bcr-Abl mutations (including T315I).[22] We decided to get further insights into this type of compounds with the aim of obtaining other active derivatives and of evaluating their activity in vivo.

In the present work, we describe the rational development of novel pyrazolo[3,4-*d*]pyrimidines able to inhibit the Bcr-Abl T315I mutant both in vitro and in vivo. A combination of in silico and in vitro studies highlighted the importance of a bromine atom in the para position of the N1 side chain phenyl ring for the interaction with the hydrophobic region I of the T315I mutant. Following this computational study, we synthesized a small collection of 4-bromo derivatives, which led to the identification of compound **2j** as the most promising inhibitor showing significant reduction of tumor volume in mice inoculated with 32D-T315I cells.

RESULTS AND DISCUSSION

Computational Studies on Bcr-Abl T315I Mutant. A cross-docking approach was employed in this study for the in silico screening of our in-house library of pyrazolo[3,4-*d*]pyrimidines (consisting of about 300 structurally characterized compounds with purity >98%) to select the most promising potential binders of the Bcr-Abl T315I mutant for biological investigation. Two crystal structures were used for this purpose, the structure of the T315I mutant of Abl kinase bound by the pyrrolo-pyridine inhibitor **3** (PPY-A) (Figure 1) (1.95 Å resolution, PDB code 2Z60)[23] and that of the T315I mutant Abl kinase domain in complex with another pyrrolo-pyridine **4** (SX7) (2.01 Å resolution, PDB code 3DK7).[24] In

dx.doi.org/10.1021/jm400233w | *J. Med. Chem.* 2013, 56, 5382−5394

contrast to other inhibitors cocrystallized with the T315I Abl mutant, such as danusertib (PHA-739358),[25] ponatinib (AP24534),[26] 5-[(5-{[4-{[4-(2-hydroxyethyl)piperazin-1-yl]-methyl}-3-(trifluoromethyl)phenyl]carbamoyl}-2-methylphenyl)ethynyl]-1-methyl-1*H*-imidazole-2-carboxamide (AP24589),[27] and rebastinib (DCC2036),[28] compounds **3** and **4** have a shape that more closely resembles that of our pyrazolo[3,4-*d*]pyrimidine compounds, including **1a**,**b** (Figure 1).

Compounds analyzed herein are already known dual Src/Abl inhibitors with activity ranging from 0.02 to 100 μM. From a structural point of view, these compounds are related to the Src inhibitors PP1 and PP2 but bear a different substitution pattern on the position 1, 3, 4, and 6 of the pyrazolo[3,4-*d*]pyrimidine nucleus. In agreement with our previously reported simulations,[20] docking studies within the ATP binding site of T315I Abl gave two different outcomes depending on the presence or the absence of an alkylthio substituent at position 6 of the pyrazolo-pyrimidine ring. Docking calculations on the C6-substituted compounds within the ATP binding site of the T315I Abl mutant did not converge to a reasonable solution, while profitable contacts could be established by the same compounds within the wild-type enzyme, in agreement with the binding mode described elsewhere.[29] Unfavorable binding poses within the T315I Abl catalytic pocket were due to the steric hindrance caused by the residue Ile315, which precludes the access of the C6-substituted pyrazolo[3,4-*d*]pyrimidines, as shown by our earlier results.[20] Instead, a well-defined binding mode was found for C6-unsubstituted compounds within the two X-ray structures of T315I Abl mutant used for calculations (Figure 2A). In detail, the C6-unsubstituted derivatives are involved in two hydrogen bonds with the Met318 of the hinge region by means of the atom N5 and the exocyclic amino group at C4. Moreover, the N1 side chain is located within a hydrophobic pocket formed by residues Lys271, Met290, Phe382, Ile313, Ile315, Val299, Val256, and Tyr253 (hydrophobic region I), while substituents at C4 interact with Leu248, Gly321, and Phe317 (hydrophobic region II). Because the amino acid in position 315 belongs to the hydrophobic region I, where the interactions between the C6-unsubstituted-pyrazolo-pyrimidines and the protein are exclusively hydrophobic, its mutation to isoleucine does not affect the correct placement of the C6-unsubstituted derivatives within the binding site. As a consequence, the binding mode proposed for the compounds within the T315I Abl binding pocket is the same of that previously found in the wild-type enzyme.[29] Comparable results were obtained using the two proteins 2Z60 and 3DK7 in terms of both chemscore values and docking poses. Examination of the results indicated that all the inhibitors showed chemscore values ranging from 25 to 37 and from 26 to 38 in 2Z60 and 3DK7, respectively. However, slight differences between the two X-ray structures were observed in the interaction of C6-unsubstituted ligands with hydrophobic region I (Figure 2B). While in 2Z60 the ligand adopted an extended conformation with the *N*1-2-chloro-2-phenylethyl substituent immersed in the deep pocket, in 3DK7, the N1-side chain was rotated by ~50° with the terminal phenyl group exposed to the solvent. The different placement of the substituent at N1 in the two crystallographic structures was mainly due to the different conformation adopted by the conserved DFG motif that affects the shape of the pocket and consequently the pattern of interactions between the N1 side chain and the protein.

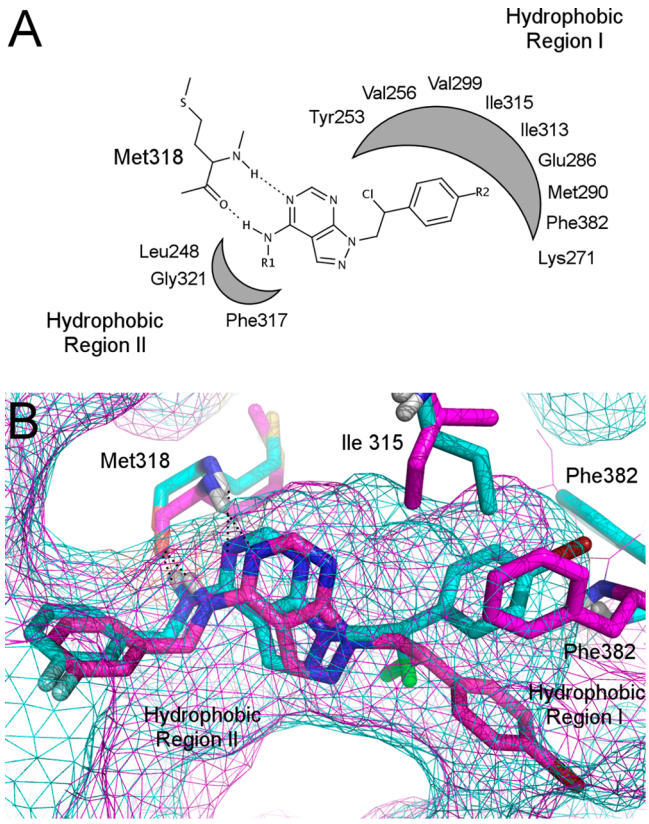

Figure 2. (A) Schematic representation of the binding mode of C6-unsubstituted pyrazolo[3,4-*d*]pyrimidines within the T315I Abl mutant binding site. (B) Binding mode of compound **2b** within 2Z60 (cyano) and 3DK7 (magenta) structures. Slight differences can be observed in the orientation of the ligand within the hydrophobic region I of the two structures.

According to the above-described docking results, the in-house available C6-unsubstituted compounds **2a**−**e** were selected for in vitro evaluation against the isolated T315I Abl together with compound **1b**, used as a reference (Table 1). These compounds were selected for testing according to the predicted score values, the number of clusters obtained, the binding poses observed, and their molecular structure in order to evaluate the importance of the R_2 substituent. Biological results are reported in Table 1. It is noteworthy that compound **2b**, in which R_2 is a bromine atom, proved to be the most active against the T315I Abl mutant (36 nM) with a comparable activity against Abl wild-type (55 nM). To rationalize these biological data, the binding free energies between Abl T315I and ligands (**1b** and **2a**−**e**) were calculated by employing the molecular mechanics/generalized Born surface area (MM-GBSA) scoring method on the docking poses (Table S2, Supporting Information). Two interesting aspects emerged from this analysis: (a) all compounds had a higher affinity for protein 2Z60 (compared to 3DK7) giving more stable complexes; (b) the ΔG values obtained with the use of 2Z60 structure better correlate with the experimental activities. In fact, the lowest binding energy (−53.2 KJ/mol) was found for compound **2b**, the most active of the series. On the other hand, no correlation between calculated and experimental data was obtained by using the 3DK7 structure. Overall, these results highlighted that 2Z60 was the most reliable structure for in silico studies on our pyrazolo-pyrimidine inhibitors and thus we decided to use only this one in the following calculations.

dx.doi.org/10.1021/jm400233w | *J. Med. Chem.* 2013, 56, 5382−5394

Table 1. Enzymatic Activities, Cellular Activities, and ADME Properties

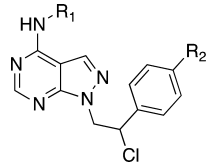

			K_i (μM)[a]			IC$_{50}$ (μM)[b]					
compd	R_1	R_2	Abl (WT)	Abl (T315I)	c-Src	P210	parental	T315I	PAMPA[c] P_{app} 10^{-6} cm/s (%MR)[d]	solub H_2O (μg mL^{-1})	met stab human (%)[e]
1b	$CH_2C_6H_4$-4F	Cl	0.08	0.16	0.8	2.7	0.5	3.0	16.6 (64)	<0.01	94.0
2a	C_6H_4-3F	F	0.732	2.430	0.160	>10	>10	1.7	13.9 (5.4)	0.03	92.3
2b	$CH_2C_6H_4$-3F	Br	0.055	0.036	0.045	3.1	>10	0.91	ND	<0.01	ND
2c	$CH_2C_6H_4$-3F	F	0.1	23.6	1.5	ND	ND	ND	ND	ND	ND
2d	$CH_2C_6H_4$-3F	H	0.04	16.7	0.08	ND	ND	ND	ND	ND	ND
2e	C_6H_4-3Cl	F	0.18	2.69	1.4	7.5	>10	3.8	ND	<0.01	ND
2f	C_6H_4-3Br	F	0.656	3.24	0.340	>10	>10	3.3	6.8 (29.3)	0.04	97.2
2g	C_6H_4-3Br	H	0.260	1.280	0.395	7.2	>10	1.7	3.20 (60)	<0.01	96.8
2h	C_6H_4-3F	H	1.440	3.000	2.350	>10	>10	8.3	7.5 (29.5)	0.08	98.0
2i	C_6H_5	H	0.89	37.5	0.11	ND	ND	ND	ND	ND	ND
2j	C_6H_5	Br	0.610	0.090	0.064	2.1	>10	0.12	6.64 (32.1)	0.06	96.4
2k	$CH_2C_6H_5$	Br	1.308	0.575	0.618	ND	ND	ND	ND	ND	ND
2l	$CH_2C_6H_4$-3Cl	Br	0.021	0.970	0.070	4.7	>10	4.5	9.1 (23.3)	<0.01	92.4
2m	$CH_2C_6H_4$-2Cl	Br	0.005	0.002	0.620	0.8	>10	0.22	8.78 (21)	<0.01	95.2
2n	$CH_2C_6H_4$-4Cl	Br	0.140	0.029	0.006	ND	ND	ND	4.24 (45.8)	<0.01	93.8
2o	$CH_2C_6H_3$-2,5Cl	Br	3.342	1.5	0.610	ND	ND	ND	ND	ND	ND
2p	$CH_2C_6H_3$-3,4Cl	Br	1.100	0.497	0.500	ND	ND	ND	ND	ND	ND
2q	$CH_2C_6H_4$-4F	Br	2.530	0.006	1.080	3.1	>10	0.15	10.7 (21.8)	<0.01	95.3
2r	$CH_2C_6H_3$-2,5F	Br	2.719	1.080	0.165	ND	ND	ND	ND	ND	ND
2s	$CH_2C_6H_3$-3,4F	Br	NA	2.710	1.700	ND	ND	ND	ND	ND	ND
2t	$CH_2C_6H_4$-4Br	Br	3.000	0.099	1.097	ND	ND	ND	3.41 (50.7)	<0.01	95.0
2u	$CH_2C_6H_4$-2Br	Br	NA	1.343	0.723	ND	ND	ND	ND	ND	ND
2v	$CH_2C_6H_4$-3Br	Br	1.264	0.673	0.770	ND	ND	ND	ND	ND	ND
2w	$CH_2C_6H_4$-3OCH_3	Br	4.750	3.400	0.150	ND	ND	ND	ND	ND	ND
2x	$CH_2C_6H_3$-3,5CF_3	Br	1.810	1.155	0.637	ND	ND	ND	ND	ND	ND
2y	C_6H_5	CH_3	0.060	1.900	ND	ND	ND	ND	ND	ND	ND
2z	C_6H_5	I	0.050	0.580	ND	ND	ND	ND	ND	ND	ND

[a]Values are the mean of at least two experiments. [b]IC$_{50}$ values are means ± SEM of series separate assays, each performed in triplicate. [c]PAMPA see Experimental Section for details. [d]Membrane retention (MR) expressed as percentage of compound unable to reach the acceptor compartment. [e]Expressed as percentage of unmodified parent drug.

Next, we focused our attention on compounds **2b**, **2c**, and **2d**, which differ only for the R_2 substituent on the N1 side chain phenyl ring (Br, F, H, respectively). To study the contribution of the bromo substituent to the activity of compound **2b**, a detailed analysis of the binding site of 2Z60 was performed with the aim of identifying regions of favorable interactions between the protein and halogen atoms (Br, F, and Cl, respectively). For this purpose, molecular interaction fields (MIFs) were calculated for the binding site by means of the software Grid.[30] Docking results and Grid analysis were then combined together. Figure 3 shows the computed binding mode of compound **2b** together with the most favorable interaction point determined for the probe Br (organic bromine atom, dark-red sphere) within the binding site of the 2Z60 protein. Interestingly, this minimum grid point is characterized by a significant favorable energy (−10.42 kcal/mol) and is located in proximity of the bromo substituent of the inhibitor **2b**. In the same position, a point of profitable interaction was also found by using the probe F. An energy of −4.34 higher than that found with Br was associated with this minimum. Interestingly, a minimum grid point for F with an energy of −3.68 kcal/mol was also found around the meta position of benzyl group at C4.

Concerning the minimum grid points calculated for probe Cl (organic chlorine atom), the most profitable interaction (−8.43 kcal/mol) was identified near the aliphatic chlorine atom of the N1-substituent. Moreover, a minimum grid point for Cl with an energy of −5.28 kcal/mol was found around the meta position of the N1 side chain phenyl ring while no minima were identified in proximity of the para position. Overall, docking results in combination with Grid analysis and MM-GBSA rescoring were able to explain the better inhibitory activity against T315I Abl mutant of compound **2b** substituted with a bromine atom in para position of the N1 side chain phenyl ring. On this basis, we decided to synthesize a small library of compounds bearing a 2-(4-bromophenyl)-2-chloroethyl N1 side chain and different amines at C4. Remarkably, a good correlation was found between calculated free energy of binding and experimental K_i toward the T315I mutant (Table S2, Supporting Information). To quantitatively study the bromine contribution to the affinity for T315I Abl mutant, Monte Carlo/free-energy perturbation (MC/FEP) calculations were

dx.doi.org/10.1021/jm400233w | J. Med. Chem. 2013, 56, 5382−5394

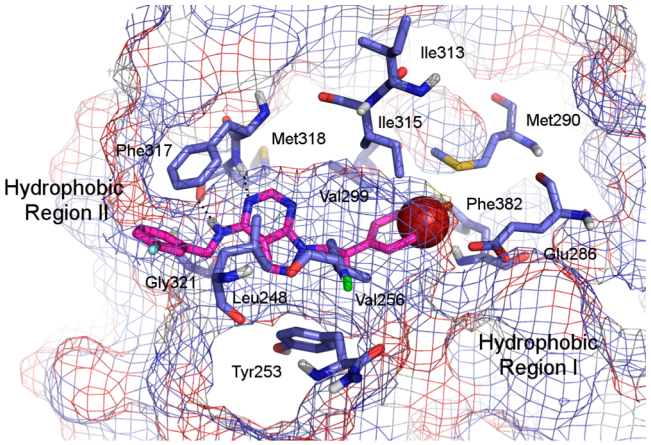

Figure 3. Binding mode of compound **2b** (*R* enantiomer) within the T315I Abl binding site. Compound locates the N1 side chain and the C4-substituent in hydrophobic region I and II, respectively. It also establishes two hydrogen bonds with Met318, involving the C4 amino group and the N5 of the pyrazolo[3,4-*d*]pyrimidine nucleus. The most favorable interaction point determined for probe Br is visualized as a red sphere. It falls in the hydrophobic region I and exactly in the region where the Br substituent of **2b** takes place.

performed to obtain computed changes in the free energy of binding for the presence of a bromine atom in the para position of the N1 chain phenyl ring. The experimental data showed that the addition of a bromo substituent in such a position is crucial, transforming a poorly active compound into an active one with a K_i of 0.090 μM (compare **2i** with **2j**, Table 1).

The MC/FEP calculations for the conversion of **2j** into **2i** gave consistent results, favoring the binding of **2j** to the T315I mutant by 2 ± 0.2 kcal/mol. Introduction of the *para*-Br substituent is computed to be particularly favorable as it projects into a hydrophobic region lined by the side chains of Ile313, Ile315, Met290, Phe382, and Glu286. Conversely, the introduction of a para fluorine into the *N*1-phenylethyl side chain had only little effect on K_i passing from 3 to 2.4 μM (compare **2h** with **2a**, Table 1). Accordingly, the replacement of hydrogen by fluorine in that position was predicted to be favorable (more negative free energy of binding) by only 0.42 ± 0.1 kcal/mol.

These results confirmed the importance of the bromine atom in para position of the N1 side chain phenyl ring for the interaction with the hydrophobic region I in the T315I mutant.

In addition, taking into account the presence of the Glu286 residue in proximity of the para position of the N1 side chain together with information obtained by SAR studies, we hypothesized that a halogen bonding[31] contribution could occur in the stabilization of the inhibitors' binding. Such interaction becomes more favorable in progressing from F to Cl to Br. An optimal distance of ca. 3.1 Å was found between the bromine atom of compound **2j** and the closest carboxyl oxygen of Glu286 during Monte Carlo FEP simulations. To better investigate this aspect, we synthesized and tested the **2j** analogues **2y** and **2z**, in which the bromine atom was replaced with a methyl group or a iodine atom, respectively. In cell-free assays, compounds **2y** and **2z** showed a lower affinity toward T315I compared with the parent *p*-Br substituted compound **2j**. Although the iodo-derivative **2z** should give a halogen bonding contribution in the binding to the T315I mutant, the bulky nature of the iodine atom determines an unfavorable binding mode that justifies the lower activity of **2z**. On the other side, the weaker binding affinity of the methyl derivative **2y** could be due to both electronic and steric reasons.

Chemistry and ADME Properties. Compounds **2e–j** and **2y,z**, bearing an anilino group in C4, were obtained in yields ranging from 57 to 71% by reacting the corresponding 4-chloro derivatives **5a–e** with an excess of the suitable aniline in absolute ethanol at reflux for 3–5 h. On the other side, the benzylamino derivatives **2k–x** were obtained in good yield by reacting the intermediate **5c** with an excess of the more nucleophilic benzylamines in anhydrous toluene at room temperature for 48–72 h (Scheme 1).

Scheme 1[a]

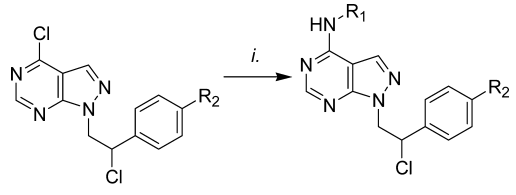

5a-e
5a: R_2 = H
5b: R_2 = F
5c: R_2 = Br
5d: R_2 = Me
5e: R_2 = I

2a-z

[a]Reagents and conditions: (i) anilines, ethanol, reflux, 3–5 h (method A); benzylamines, toluene, rt, 48–72 h (method B).

The synthesis of intermediates **5a–c** was previously performed by us, using as starting products the suitable phenyloxiranes and hydrazine monohydrate.[17b] The synthesis of intermediates **5d,e** was performed by us using a different route because the corresponding oxiranes are not commercially available. Allopurinol **6** was chlorinated with $POCl_3$/DMF and successively substituted on N1 with the suitable 2-bromoacetophenone, in the presence of TBAF as a base, affording intermediates **8a,b**. Reduction of these compounds with sodium borohydride led to the corresponding alcohols **9a,b** that were finally chlorinated to **5d,e** (Scheme 2).

The most interesting compounds identified by the biological assays were then submitted to a thorough in vitro ADME study to determine their aqueous solubility, parallel artificial membrane permeability (PAMPA), and human liver microsomes (HLM) stability in order to early assess the absorption/stability of these drug candidates (Table 1). Passive membrane permeability was evaluated with the PAMPA assay, applying a validated protocol recently developed by us for poorly water-soluble pyrazolo[3,4-*d*]pyrimidines.[32] Although the presence of a cosolvent (DMSO) proved to slightly decrease the penetration of the compounds, a good correlation was found with the experimental data, and overall, this protocol gives useful insights in ranking the intestinal absorption of lipophilic compounds. Compound solubility was then evaluated following the method developed by Avdeef et al., and results were expressed in μg/mL.[33] Metabolic stability was finally evaluated by incubating the above-mentioned compounds with 5 μL of man-pooled HLM for 1 h at 37 °C in order to simulate phase I metabolism. The parent drugs and metabolites were subsequently determined by LC-MS analysis.

In general, the synthesized compounds showed values of membrane permeation and metabolic stability comparable to that of the reference **1b** but, in most of the cases, they displayed

dx.doi.org/10.1021/jm400233w | *J. Med. Chem.* 2013, 56, 5382–5394

Scheme 2[a]

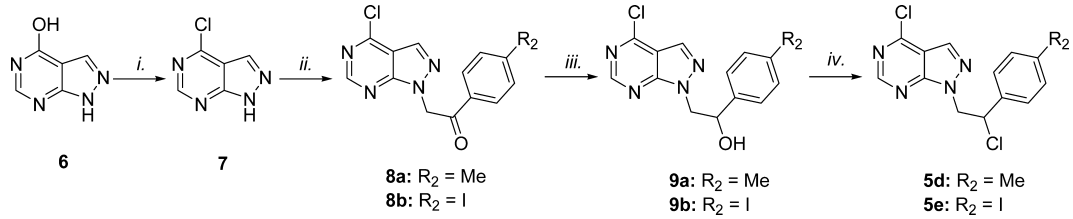

[a]Reagents and conditions: (i) $POCl_3$/DMF reflux, 12 h; (ii) TBAF 2M in THF, $BrCH_2COC_6H_4R_2$, THF, rt, 24 h; (iii) $NaBH_4$, THF, 0 °C; (iv) $POCl_3$/DMF, reflux 5 h.

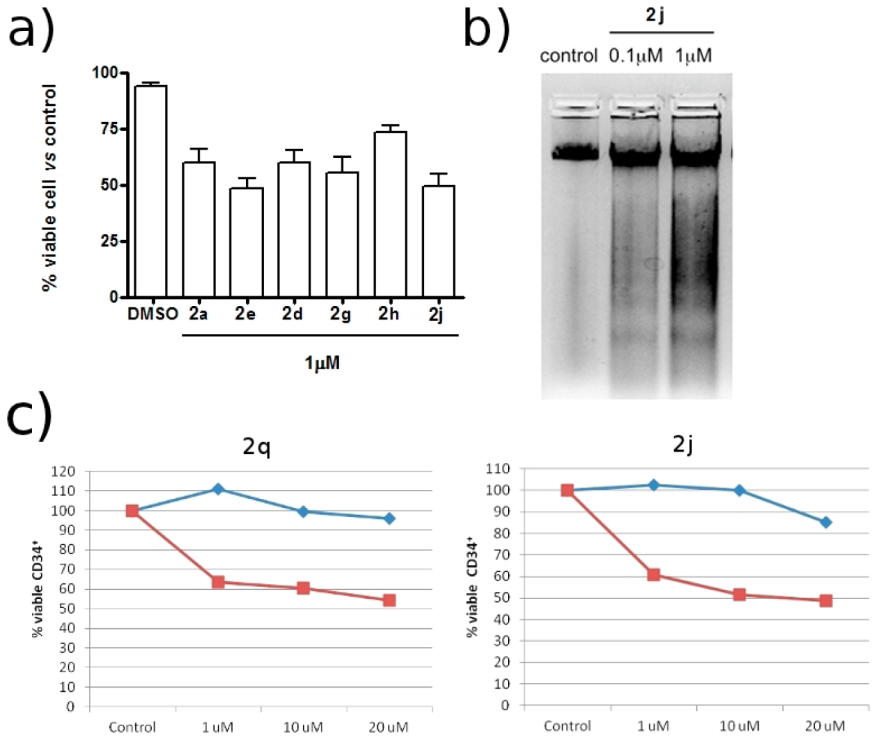

Figure 4. Cell death in response to treatment with selected inhibitors. (a) The percentage of dead cells was calculated considering the total number of 32D-T315I cells treated for 48 h with 1 μM of representative compounds. The values of three different experiments were considered to calculate the mean and the standard deviation. (b) Agarose gel electrophoretic analysis of genomic DNA extracted from 32D-T315I cells treated for 48 h with 0.1 and 1 μM **2j** in comparison with untreated cells (control). (c) Percentage of CD34+ cells from bone marrow samples of CML (blu lines) and T315I CML patients (red lines) after treatment with **2q** (left) and **2j** (right).

a lower membrane retention (Table 1, data in parentheses). The ADME investigation highlighted good metabolic stability (higher than 90%) and membrane permeability (ranging from 3.20 to 13.9 × 10^{-6} cm/s) for the most representative compounds, while the water solubility was in the medium−low range. A few compounds (**2a**, **2f**, **2h**, and **2j**) presented however a better water solubility with respect to the reference compound **1b**.

In Vitro Biological Activity. All the synthesized compounds were initially tested in a cell-free assay to evaluate their affinity toward Abl, Abl T315I mutant, and Src enzymes in comparison with the reference compound **1b**, which was previously reported to inhibit Ba/F3 cells expressing the Bcr-Abl T315I mutant.[20] As can be appreciated from Table 1, among the compounds selected by the virtual screening (**2a**−**e**), derivative **2b** showed to be a potent inhibitor of the T315I mutant. This activity was linked to the presence of the bromine atom in para position of the N1 side chain phenyl ring, as hypothesized by our molecular modeling calculations and further confirmed by comparing the activity data of **2b** with those of **2c**,**d**. All para bromo derivatives herein synthesized, with the only exceptions of **2s** and **2u**, maintained a dual Src/Abl inhibitory profile. As suggested by the molecular modeling studies, all compounds bearing a bromine atom in para position of the N1 side chain phenyl ring (**2b**, **2j**−**x**) maintained or improved the activity against the T315I mutant. Among these derivatives, compounds **2b**, **2j**, **2m**, **2n**, **2q**, and **2t** showed a high affinity for Abl T315I, with a K_i in the nanomolar range (36, 90, 2, 29, 6, and 99 nM, respectively) while the affinity for the wild-type Abl was generally in a lower range (55, 610, 5, 140, 2530, and 3000 nM, respectively). Selected compounds (**2a**,**b**, **2e**−**h**, **2j**, **2l**−**m**, and **2q**) were then evaluated for their in vitro cytotoxic effect using the murine myeloid cell line 32D expressing the nonmutated Bcr-Abl fusion protein (p210) or the mutated form T315I. Cells were treated for 48 h with increasing concentrations of the inhibitors (0.01−50 μM), and IC_{50}s were calculated by considering the number of vital cells with respect to the control (Table 1). Notably, all the tested

dx.doi.org/10.1021/jm400233w | J. Med. Chem. 2013, 56, 5382−5394

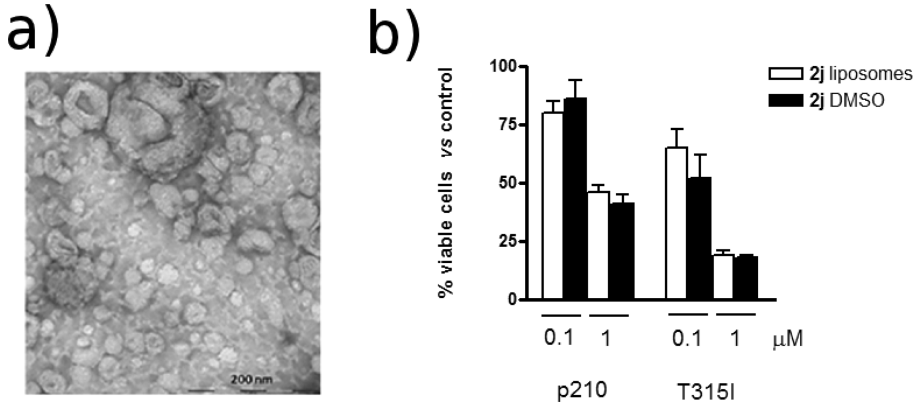

Figure 5. Liposomes formulation experiments. (a) TEM image of negative stain liposomes loaded with **2j**; SUV (<200 nm) are clearly visible. (b) Myeloid cells, 32D-p210, and 32D-T315I (p210 and T315I) were treated with **2j** (0.1 and 1 μM) prepared in DMSO or encapsulated in liposomes and cell viability was measured after 48 h of incubation. The values of three different experiments were considered to calculate the mean and the standard deviation.

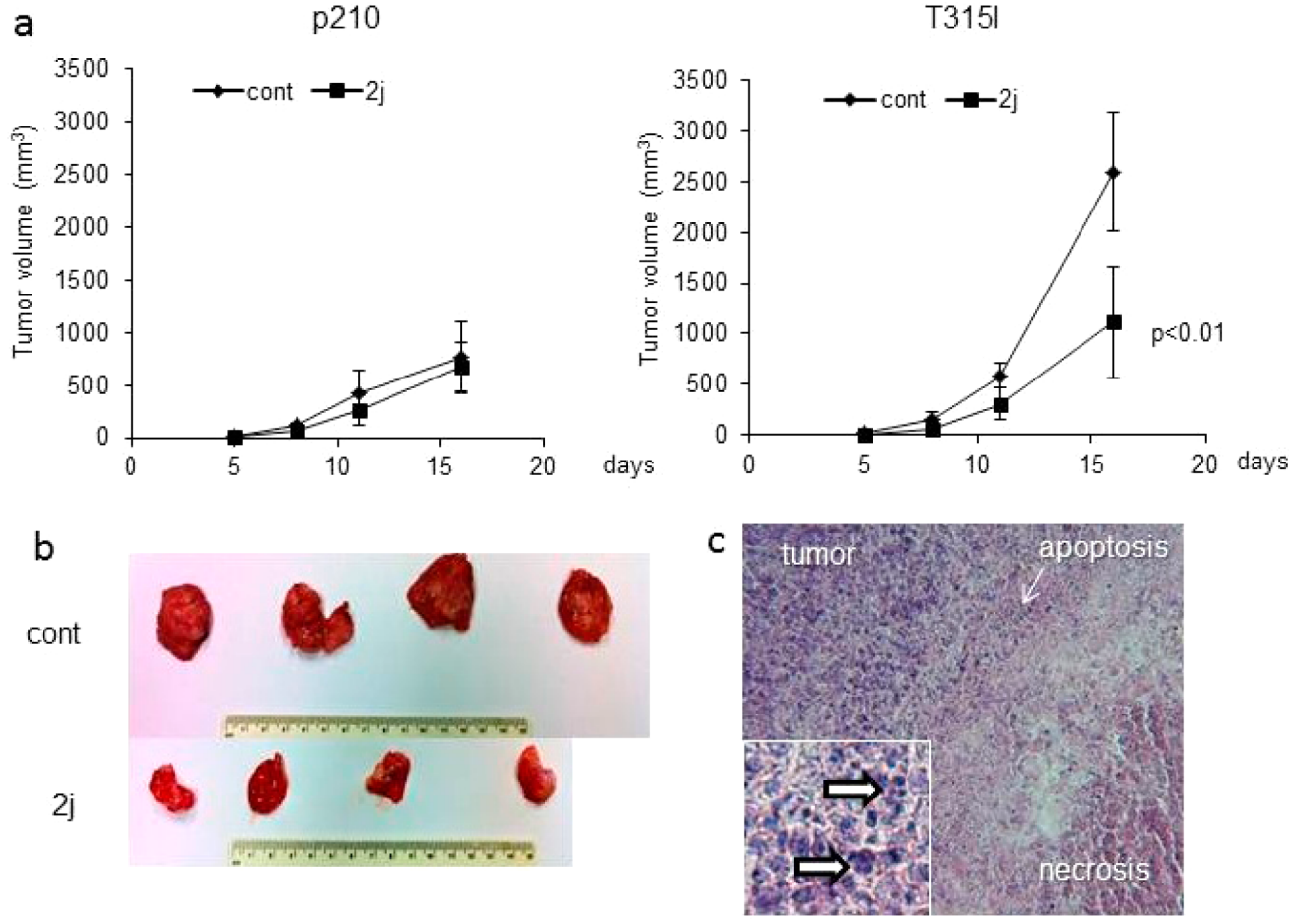

Figure 6. (a) Nude mice were inoculated sc with 32D-p210 or 32D-T315I cells, and tumor growth was monitored by measuring tumor mass width and length. For each cell line inoculated, mice were divided in a control group and a **2j**-treated group, with each group represented at least by five mice. $P < 0.01$ according to Student's t test. (b) At the end point of the experiment in (a), tumor masses were excised from mice inoculated with 32D-T315I cells. Representative tumor masses from each experimental group are shown. (c) Histological image taken from 32D-T315I graft treated with **2j**, showing a necrotic area within the tumor. A region containing apoptotic figures is evident in the boundary of the necrotic zone (white arrow). In the inset, a magnification image illustrating the apoptotic figures is shown.

compounds showed a higher cytotoxic activity against IM-resistant cells expressing T315I mutated Bcr-Abl compared to IM-sensitive 32D-p210 cells, in partial accordance with the enzymatic data. In 32D-T315I cells, IC_{50}s ranged from 0.12 to 8.3 μM and compounds demonstrated different capacities in inducing cell death. When 32D-T315I cells were treated for 48 h with 1 μM of the compounds, cell death was observed for all compounds analyzed and the number of dead cells was higher than 50% of the total only for **2e**, **2g**, and **2j** (Figure 4a). Apoptosis was the prevalent modality of death as indicated by

dx.doi.org/10.1021/jm400233w | J. Med. Chem. 2013, 56, 5382−5394

the ordered fragmentation of genomic DNA (Figure 4b). In addition, it was noteworthy that these 4-bromo derivatives did not show cytotoxic effects when tested up to 10 μM concentration in parental cell lines (see Table 1) which did not express the chimeric Bcr-Abl protein. Furthermore, compounds **2q** and **2j** were also tested on early hematopoietic progenitors (CD34+) from Ph^+ CML patients at diagnosis and from Ph^+ CML patients who developed resistance to Imatinib mesylate in consequence of T315I Bcr-Abl mutation. Cells were seeded at 4×10^5 cells/mL density and treated with **2q** and **2j** and with DMSO vehicle control at concentrations of 1, 10, and 20 μM for 48 h. In Ph^+ T315I mutant CML cells, the percentage of viable cells after treatment with the two compounds decreases with increasing compound concentration. By contrast, in Ph^+ CML cells, no effects were observed (Figure 4c).

Most of the compounds present therefore an activity profile complementary to that of IM, dasatinib, and other known Abl inhibitors, being inhibitors of cell lines expressing the T315I Bcr-Abl construct with a moderate effect on IM-sensitive cells. Among the most promising T315I inhibitors, compounds **2j** was selected for the in vivo studies because it showed a good balance of different ADME properties, high activity in cell-free assays, and interesting submicromolar potency against T315I Bcr-Abl expressing cells at the same time. An important issue for a potential in vivo application in cancer therapy of a novel agent effective in vitro at relatively high dosage is represented by the design of a suitable drug formulation, characterized by a prolonged blood half-life and a good biocompatibility. The use of DMSO as solubilizing agent for drugs with a lower solubility would be not suitable for clinical settings. According to these considerations, liposome formulation of **2j** was prepared for in vitro screening in order to check if the activity profile could be improved by a further increase of water solubility. The small unilamellar vesicle (SUV) liposomes were characterized by negative stain transmission electron microscopy (TEM) for vesicle morphology and size (Figure 5a). Entrapment efficiency was calculated with HPLC-UV analysis showing a good entrapment efficiency (>98%).

Liposome encapsulated **2j** was tested on 32D-p210 and 32D-T315I cells at concentrations 0.1 and 1 μM in comparison with the DMSO dissolved **2j** at the same concentration (Figure 5b). The cytotoxic effect of liposome encapsulated **2j** at both concentrations was almost the same as that of **2j** dissolved in DMSO. This result is important because it shows that the liposome formulation, which is completely water soluble, can avoid the use of DMSO as a solubilizing agent to test our poorly water-soluble pyrazolo-pyrimidines.

In Vivo Studies. The antitumor activity of **2j** was finally tested in vivo using a xenograft mouse model. Mice inoculated with 32D-p210 or 32D-T315I cells were treated daily with 80 mg/kg **2j** starting from the appearance of a visible tumor mass, and the tumor volume was evaluated at regular intervals. **2j** caused a significant reduction in tumor volumes after 17 days of treatment only in mice inoculated with 32D-T315I cells, with a reduction of more than 50% in mean tumor volume compared to placebo treated mice (Figure 6a, right graph). In mice inoculated with 32D-p210 cells, we observed a reduction in mean tumor volume after treatment with **2j**, mainly in the first week, but this difference was not statistically significant (Figure 6a, left graph). It is notable that 32D-p210 cells had a slower growing rate in vivo with respect to 32D-T315I, and this aspect further demonstrated the effectiveness of **2j** in a very aggressive tumor model. The antitumor effect of **2j** was evident when comparing tumor masses excised from mice at the end of the experiment (Figure 6b). The tumors from mice inoculated with 32D-T315I were analyzed by routine histology methods and revealed the presence of a significant amount of necrotic tissue component in mice treated with **2j**. In particular, in these tumors, apoptotic zone flanking necrotic areas resulted and were clearly visible (Figure 6c).

CONCLUSIONS

Starting from our internal collection of pyrazolo[3,4-*d*]-pyrimidines, a cross-docking approach allowed identification of a point modification, consisting in placing a bromine atom on the para position of the N1 side chain phenyl ring as a key feature to establish profitable interactions with the hydrophobic region I in Abl T315I mutant. Results of the docking studies in combination with Grid analysis, MM-GBSA rescoring, and MC/FEP calculations were in fact able to explain the important role played by such 4-Br derivatives in the binding to the T315I Abl mutant. A small collection of pyrazolo[3,4-*d*]pyrimidines (**2j**−**x**) bearing this 4-bromo substitution on the N1 side chain phenyl ring was thus synthesized and tested in cell-free assays against Abl, Src, and Abl T315I; as expected, **2j**−**x** maintained or improved the activity against the T315I mutant.

All 4-bromo derivatives herein synthesized, with the only exceptions of **2s** and **2u**, maintained a dual Src/Abl inhibitory profile. As suggested by the molecular modeling studies, all compounds bearing a bromine atom in para position of the N1 side chain phenyl ring (**2j**−**x**) maintained or increased the activity against the T315I mutant, compared to **2b**, while the same trend was not observed with other derivatives lacking this 4-Br substitution (**2c**−**i**).

A few compounds (**2a**, **2f**, **2h**, and **2j**) showed superior ADME properties, when compared with the reference compound **1b**, and were further investigated for their in vitro cytotoxic effect using the murine myeloid cell line 32D expressing the nonmutated Bcr-Abl fusion protein (p210) or the mutated form T315I. An interesting submicromolar potency against T315I Bcr-Abl expressing cells was found without any cytotoxic effects when tested up to 10 μM concentration in parental cell lines. Most of the compounds present therefore an activity profile complementary to that of IM, dasatinib, and other known Abl inhibitors, being better inhibitors of cell lines expressing the T315I Bcr-Abl construct with a moderate effect on IM-sensitive cells. Finally, in vivo studies on mice inoculated with 32D-T315I cells and treated with **2j** showed a significant reduction (more than 50%) of tumor volumes with respect to placebo treated mice. In conclusion, compound **2j** represents an improved pyrazolo[3,4-*d*]pyrimidine analogue active in vivo on the Bcr-Abl T315I mutant and therefore worthy of further investigation.

EXPERIMENTAL SECTION

Computer Modeling. *Docking Studies.* Docking studies of all pyrazolo[3,4-*d*]pyrimidine derivatives were performed within the ATP binding site of the T315I Abl mutant (PDB code 2Z60 and 3DK7) using the software package Gold 4.1.[34] Compounds were first processed with the Schrodinger LigPrep tool to generate separate files for all possible enantiomers and protonation states at physiological pH. The protein structures were prepared using the Protein Preparation Wizard in the Schrodinger software graphical user interface Maestro (version 9.1).[35] Chemscore was chosen as the fitness function for docking calculation with the CHO_TYPE term set to SPECIAL to enable the recognition of activated CH groups for

dx.doi.org/10.1021/jm400233w | J. Med. Chem. 2013, 56, 5382−5394

hydrogen bonding. The genetic algorithm parameter settings were employed using the search efficiency set at 100%, and 100 runs were carried out for each ligand. The reliability of the docking protocol was first checked by simulation of the interactions between **3** and **4** with the two crystal structures of the Abl T315I mutant and comparison of the modeled complexes with the X-ray data. As a results, compounds **3** and **4** showed in both proteins an orientation in agreement with their binding orientation and interactions onto the relative X-ray structure. Taken together, these results led us to hypothesize that the computational approach can be considered as a reliable modeling procedure to be applied for finding the orientations and interactions of ligand inside the kinase domain of T315I Abl mutant.

MM-GBSA. To remove unfavorable contacts, protein−ligand complexes were imported in Maestro 9.1 and minimized through the OPLS-AA force field and Polak−Ribiere conjugate gradient method (0.05 KJ/mol·Å convergence or 200 iterations). A continuum solvation method, with water as the solvent, was applied. Next, to rescore ligands, MM-GBSA calculations of free energy of binding were performed using the program Prime in Maestro suite from Schrödinger.[35]

MIF Analysis. Computation of MIFs within the ATP binding pocket of Abl T315I was carried out with the software Grid.[30] Box dimensions were defined so as to accommodate all the residues constituting the binding site and the number of planes of grid points per Angstrom (NPLA) parameter was set to 1. MIFs were computed for Br, Cl, and F probes. To achieve the points of minimum of MIFs, Grid calculations were performed for each probe separately and using the export GRIDKONT option. The kont files corresponding to each MIF were then processed by means of the minim and filmap programs (both implemented in the Grid package) that extract all the points of minimum of each MIF and retain only those falling under a user-defined cutoff.

Free Energy Perturbation. MC/FEP[36] calculations were performed with the MCPRO[37] program and followed standard protocols.[38,39] *Z*-Matrix for the protein−ligand complexes, and free ligands were obtained with the molecular growing program BOMB[36] starting from the docking pose of compound **2j**. A conformational search was then carried out on the ligands using the BOSS[37] program with the OPLS/CM1A force field and GB/SA hydration. The resultant conformer with the lowest-energy was used for FEP calculation. The unbound ligands and complexes were solvated in TIP4P water spheres ("caps") with a 25 Å radius; after the removal of water molecules in too close contact with solute atoms, ca. 2000 and 1250 water molecules remained for the unbound and bound MC simulations. All protein residues within ca. 15 Å of any ligand atom were included. A few remote side chains were neutralized in order to maintain overall charge neutrality for each system. The ligand and the protein side chains within 10 Å of any ligand atoms were sampled during the MC simulations. The only constraints were the bond lengths in side chains, and all backbone atoms were frozen after a short conjugate-gradient minimization. The energetics for the systems were evaluated with the OPLS-AA force field for the protein and OPLS/CM1A for the ligand.[40] As usual, the CM1A atomic charges were scaled by 1.14 for neutral molecules. Differences in free energies of binding were determined from the usual thermodynamic cycle that requires conversion of one ligand to another both free in water and bound to the protein. The FEP calculations utilized 11 windows of simple overlap sampling. For the unbound ligand, each window consisted of 40 M configurations of equilibration and 60 M configurations for averaging. For the bound calculations, each window covered 20 M configurations of solvent-only equilibration, 40 M configurations of full equilibration, and 50 M configurations of averaging. All MC simulations were run at 298 K. Due to the fact that the biological evaluation of all the chiral compounds reported here was carried out using racemic mixtures, MC/FEP analysis was performed on both *R*- and *S*-enantiomers and medium values of free energy of binding was calculated.

Chemistry. Starting materials were purchased from Aldrich-Italia (Milan, Italy). Melting points were determined with a Büchi 530 apparatus and are uncorrected. IR spectra were measured in KBr with a Perkin-Elmer 398 spectrophotometer. ^{1}H NMR spectra were recorded in a $(CD_3)_2SO$ solution on a Varian Gemini 200 (200 MHz) instrument. Chemical shifts are reported as δ (ppm) relative to TMS as the internal standard, *J* in Hz. ^{1}H patterns are described using the following abbreviations: s = singlet, m = multiplet, and br s = broad singlet. TLC was carried out using Merck TLC plates silica gel 60 F254. Chromatographic purifications were performed on columns packed with Merk 60 silica gel, 23−400 mesh, for flash technique. Analyses for C, H, and N were within ±0.3% of the theoretical value. Mass spectra (MS) data were obtained using an Agilent 1100 LC/MSD VL system (G1946C) with a 0.4 mL/min flow rate using a binary solvent system of 95:5 methanol/water. UV detection was monitored at 254 nm. MS were acquired in positive and negative modes, scanning over the mass range 50−1500. The following ion source parameters were used: drying gas flow, 9 mL/min; nebulizer pressure, 40 psig; drying gas temperature, 350 °C. All target compounds possessed a purity of ≥95% as verified by elemental analyses by comparison with the theoretical values. Synthesis and analytical data of intermediates **3a−c** and compounds **2a−d** were previously reported by us.[17b,41]

*General Procedure for the Synthesis of **2e−j** and **2y,z**.* A solution of the appropriate 4-chloro derivatives **5a−c**[17b,41] or **5d,e** (1 mmol) and the suitable aniline (2 mmol) in absolute ethanol was refluxed for 3−5 h. After cooling, the solvent was evaporated under reduced pressure, and the crude was treated with water (20 mL) then extracted with CH_2Cl_2 (20 mL); the organic phases were washed with water (20 mL), dried ($MgSO_4$), and concentrated under reduced pressure. The obtained oils were crystallized by adding a mixture of diethyl ether/petroleum ether (bp 40−60 °C) (1:1) and standing in a refrigerator to afford compounds **2e−j** and **2y,z** as white solids, which were recrystallized from absolute ethanol.

*1-[2-Chloro-2-(4-fluorophenyl)ethyl]-N-(3-chlorophenyl)-1H-pyrazolo[3,4-d]pyrimidin-4-amine (**2e**).* White solid (273 mg, 68%); mp 186−187 °C. ^{1}H NMR: δ 4.62−4.78 and 4.83−4.98 (2m, 2H, CH_2N), 5.38−5.49 (m, 1H, CHCl), 6.86−7.47 (m, 8H Ar), 7.57 (s, 1H, H-3), 8.37 (s, 1H, H-6). IR cm^{-1}: 3168 (NH). MS: *m*/*z* 402 [M + H]$^+$. Anal. ($C_{19}H_{14}N_5Cl_2F$) C, H, N.

*General Procedure for the Synthesis of **2k−x**.* To a solution of 1-[2-(4-bromophenyl)-2-chloroethyl]-4-chloro-1*H*-pyrazolo[3,4-*d*]-pyrimidine **5c**[41b] (1 mmol, 372 mg) in anhydrous toluene (10 mL), the suitable amine (4 mmol) was added and the mixture was stirred at room temperature for 48−72 h. Then the organic phase was washed with water (2 × 10 mL), dried ($MgSO_4$), and concentrated under reduced pressure. The crude oils were crystallized by adding a mixture of diethyl ether/petroleum ether (bp 40−60 °C) (1:1) and standing in a refrigerator to afford compounds **2k−x** as white solids, which were recrystallized from absolute ethanol.

*N-Benzyl-1-[2-(4-bromophenyl)-2-chloroethyl]-1H-pyrazolo[3,4-d]pyrimidin-4-amine (**2k**).* White solid (261 mg, 59%); mp 182−184 °C. ^{1}H NMR: δ 4.68−4.77 and 4.84−4.89 (2m, 4H, CH_2N + CH_2Ar), 5.42−5.45 (m, 1H, CHCl), 7.19−7.39 (m, 10H, 9Ar + H-3), 7.88 (s, 1H, H-6). IR cm^{-1}: 3210 (NH). MS: *m*/*z* 443 [M + H]$^+$. Anal. ($C_{20}H_{17}N_5BrCl$) C, H, N.

*Synthesis of 4-Chloro-1H-pyrazolo[3,4-d]pyrimidine (**7**).* Allopurinol **6** (2 g, 14.7 mmol) was added to $POCl_3$ freshly distilled (15 mL). Dry DMF (3.4 mL) was added to this mixture, and the solution was refluxed for 12 h. After cooling at room temperature, the reaction mixture was poured in a hydrogen carbonate saturated aqueous solution at 0 °C. The aqueous solution was extracted with EtOAc (50 mL). The organic phase was dried (Na_2SO_4) and concentrated under reduced pressure to obtain a yellow solid (1.72 g, 76%) used without further purification in the next step.

^{1}H NMR: δ 8.32 (s, 1H, H-3), 8.93 (s, 1H, H-6), 12.23 (br s, 1H, NH, disappears with D_2O). MS: *m*/*z* 154 [M − H]$^-$.

*General Procedure for the Synthesis of **8a,b**.* Compound 7 (200 mg, 1.29 mmol) was dissolved in dry THF (10 mL) at room temperature, and TBAF 2.0 M in THF solution (2.58 mmol) was added, following the procedure described by Brik et al.[42] The desired 2-bromoacetophenone (1.29 mmol) was added to the solution, and the reaction mixture was stirred at room temperature for 24 h. The reaction mixture was filtered on Celite pad then extracted with EtOAc

(100 mL) and water. The organic phase was dried (Na_2SO_4) and concentrated under reduced pressure. The crude was purified by flash chromatography on silica gel (eluent CH_2Cl_2/MeOH 99:1).

*2-(4-Chloro-1H-pyrazolo[3,4-d]pyrimidin-1-yl)-1-(4-methylphenyl)ethanone (**8a**).* Yellow oil (267 mg, 72%). ^{1}H NMR: δ 2.28 (s, 3H, CH_3), 5.86 (s, 2H, CH_2N), 7.13−7.15 and 7.76−7.78 (2m, 4H Ar), 8.10 (s, 1H, H-3), 8.59 (s, 1H, H-6). MS: m/z 287 $[M + H]^+$. Anal. ($C_{14}H_{11}N_4ClO$) C, H, N.

*2-(4-Chloro-1H-pyrazolo[3,4-d]pyrimidin-1-yl)-1-(4-iodophenyl)-ethanone (**8b**).* Light-brown oil (278 mg, 70%). ^{1}H NMR: δ 5.88 (s, 2H, CH_2N), 7.65−7.67 and 7.81−7.83 (2m, 4H Ar), 8.20 (s, 1H, H-3), 8.70 (s, 1H, H-6). MS: m/z 399 $[M + H]^+$. Anal. ($C_{13}H_8N_4ClIO$) C, H, N.

*General Procedure for the Synthesis of **9a,b**.* $NaBH_4$ (119 mg, 3.14 mmol) was added to a solution of **8a** or **8b** (1.57 mmol) in dry THF at 0 °C. The reaction mixture was stirred until the starting material disappeared. The reaction was quenched by adding water then it was extracted with EtOAc (50 mL). The organic phase was dried (Na_2SO_4) and concentrated under reduced pressure. The solid was purified by flash chromatography on silica gel (eluent CH_2Cl_2/MeOH 99:1).

*2-(4-Chloro-1H-pyrazolo[3,4-d]pyrimidin-1-yl)-1-(4-methylphenyl)ethanol (**9a**).* Yellow solid (290 mg, 64%); mp 85−87 °C. ^{1}H NMR: δ 2.00 (s, 3H, CH_3), 4.50−4.55 and 4.63−4.68 (2m, 2H, CH_2N), 5.16−5.19 (m, 1H, CHOH), 7.03−7.05 and 7.19−7.21 (2m, 4H Ar), 8.02 (s, 1H, H-3), 8.55 (s, 1H, H-6). MS: m/z 289 $[M + H]^+$. Anal. ($C_{14}H_{13}N_4ClO$) C, H, N.

*2-(4-Chloro-1H-pyrazolo[3,4-d]pyrimidin-1-yl)-1-(4-iodophenyl)-ethanol (**9b**).* Yellow solid (388 mg, 62%); mp 90−92 °C. ^{1}H NMR: δ 4.61−4.66 and 4.74−4.80 (2m, 2H, CH_2N), 5.21−5.24 (m, 1H, CHOH), 7.08−7.10 and 7.58−7.60 (2m, 4H Ar), 8.02 (s, 1H, H-3), 8.57 (s, 1H, H-6). MS: m/z 401 $[M + H]^+$. Anal. ($C_{13}H_{10}N_4ClIO$) C, H, N.

*General Procedure for the Synthesis of **5d,e**.* Compound **9a** or **9b** (1.06 mmol) was added to $POCl_3$ freshly distilled (10 mL). To this mixture was added DMF (3.0 mL), and the solution was refluxed for 5 h. After cooling at room temperature, the reaction mixture was poured in a hydrogen carbonate saturated aqueous solution at 0 °C. The aqueous solution was extracted with EtOAc (20 mL). The organic phase was dried (Na_2SO_4) and concentrated under reduced pressure. The reaction crude was purified by flash chromatography on silica gel (eluent Hex/EtOAc 95:5).

*4-Chloro-1-[2-chloro-2-(4-methylphenyl)ethyl]-1H-pyrazolo[3,4-d]pyrimidine (**5d**).* White solid (129 mg, 40%); mp 100−102 °C. ^{1}H NMR: δ 2.30 (s, 3H, CH_3), 4.81−4.86 and 5.02−5.08 (2m, 2H, CH_2N), 5.48−5.52 (m, 1H, CHCl), 7.11−7.12 and 7.30−7.32 (2m, 4H Ar), 8.15 (s, 1H, H-3), 8.73 (s, 1H, H-6). MS: m/z 307 $[M + H]^+$. Anal. ($C_{14}H_{12}N_4Cl_2$) C, H, N.

*4-Chloro-1-[2-chloro-2-(4-iodophenyl)ethyl]-1H-pyrazolo[3,4-d]-pyrimidine (**5e**).* Yellow solid (168 mg, 38%); mp 112−114 °C. ^{1}H NMR: δ 4.81−4.86 and 4.98−5.04 (2m, 2H, CH_2N), 5.44−5.48 (m, 1H, CHCl), 7.15−7.17 and 7.64−7.66 (2m, 4H Ar), 8.15 (s, 1H, H-3), 8.74 (s, 1H, H-6). MS: m/z 419 $[M + H]^+$. Anal. ($C_{13}H_9N_4Cl_2I$) C, H, N.

ADME Assays. *Chemicals.* All solvents, reagents, L-α-phosphatidylcholine, and cholesterol were from Sigma-Aldrich Srl (Milan, Italy). Dodecane was purchased from Fluka (Milan, Italy). Pooled Male Donors 20 mg/mL HLM were from BD Gentest-Biosciences (San Jose, California). Milli-Q quality water (Millipore, Milford, MA, USA) was used. Hydrophobic filter plates (MultiScreen-IP, clear plates, 0.45 μm diameter pore size), 96-well microplates, and 96-well UV-transparent microplates were obtained from Millipore (Bedford, MA, USA).

Parallel Artificial Membrane Permeability Assay (PAMPA). Donor solution (0.5 mM) were prepared by diluting 1 mM DMSO compound stock solution using phosphate buffer (pH 7.4, 0.025 M). Filters were coated with 5 μL of a 1% (w/v) dodecane solution of phosphatidylcholine. Donor solution (150 μL) were added to each well of the filter plate. To each well of the acceptor plate were added 300 μL of solution (50% DMSO in phosphate buffer). All compounds were tested in three different plates on different days. The sandwich was incubated for 5 h at room temperature under gentle shaking. After the incubation time, the sandwich plates were separated, and samples taken from both receiver and donor sides were analyzed using LC-UV-MS method. Permeability (P_{app}) for PAMPA, was calculated according to the equation obtained from Wohnsland and Faller.[43]

LC-UV-MS Method. Chromatographic analysis were performed with an Agilent 1100 LC/MSD VL system (G1946C) (Agilent Technologies, Palo Alto, CA) constituted by a vacuum solvent degassing unit, a binary high-pressure gradient pump, an 1100 series UV detector, and an 1100 MSD model VL benchtop mass spectrometer. Chromatographic separation was obtained using a Varian Polaris 5 C18-A column (150 mm × 4.6 mm, 5 μm particle size) and gradient elution: eluent A being ACN and eluent B consisting of an aqueous solution of formic acid (0.1%). The analysis started with 2% of eluent A, which was rapidly increased up to 70% in 10 min, then slowly increased up to 98% in 15 min. The flow rate was 1.0 mL/min, and injection volume was 20 μL. The Agilent 1100 series mass spectra detection (MSD) single-quadrupole instrument was equipped with the orthogonal spray API-ES (Agilent Technologies, Palo Alto, CA). Nitrogen was used as nebulizing and drying gas. The pressure of the nebulizing gas, the flow of the drying gas, the capillary voltage, the fragmentor voltage, and the vaporization temperature were set at 40 psi, 9 L/min, 3000 V, 70 V, and 350 °C, respectively. UV detection was monitored at 280 nm. The LC-ESI-MS determination was performed by operating the MSD in the positive ion mode. Spectra were acquired over the scan range m/z 100−1500 using a step size of 0.1 u.

Microsomal Stability Assay. Each compound in DMSO solution was incubated at 37 °C for 60 min in 125 mM phosphate buffer (pH 7.4), 5 μL of human liver microsomal protein (0.2 mg/mL), in the presence of a NADPH-generating system at final volume of 0.5 mL (compound final concentration 100 μM).[19] The reaction was stopped by cooling in ice and adding 1.0 mL of acetonitrile. The reaction mixtures were centrifuged, and the parent drug and metabolites were subsequently determined by the above-mentioned LC-UV-MS method.

Water Solubility Assay. Each solid compound (1 mg) was added to 1 mL of water. The samples were shaked in a shaker bath at 20 °C for 24−36 h. The suspensions were filtered through a 0.45 μm nylon filter (Acrodisc), and the solubilized compound determined by LC-UV-MS assay. For each compound, the determination was performed in triplicate.

Liposomal Formulation. Liposomal formulations (phosphatidylcholine/cholesterol 90:10 (w/w)) were prepared with thin layer evaporation method. Compound **2j**, lipid(s), and cholesterol were dissolved in chloroform/ethanol 3:2 (v/v), and the organic solvent was evaporated to get a dry powder. Proliposomes (powder) were hydrated in pH 7.4 phosphate buffered saline (PBS) by vortex and sonication to obtain SUV liposomes. Liposomes were characterized by negative stain electron microscopy (TEM) for vesicle morphology and size. Entrapment efficiency was calculated with HPLC-UV analysis.

Biological Studies. *Enzymatic Assay on Isolated Src.* Recombinant human Src was purchased from Upstate (Lake Placid, NY). Activity was measured in a filter-binding assay using a commercial kit (Src Assay Kit, Upstate), according to the manufacturer's protocol, using 150 μM of the specific Src peptide substrate (KVEKIGEGTYGVVYK) and in the presence of 0.125 pmol of Src and 0.160 pmol of [γ-^{32}P]-ATP. The apparent affinity (K_m) values of the Src preparation used for its peptide and ATP substrates were determined separately and found to be 30 and 5 μM, respectively.

Kinetic Analysis. Dose−response curves were generated by fitting the data by computer simulation to eq 1: $E_{(\%)} = E_{max}/(1 + [I]/ID_{50})$, where $E_{(\%)}$ is the fraction of the enzyme activity measured in the presence of the inhibitor, E_{max} is the activity in the absence of the inhibitor, $[I]$ is the inhibitor concentration, and ID_{50} is the inhibitor concentration at which $E_{(\%)} = 0.5E_{max}$. The ID_{50} were converted to K_i according to a competitive mechanism with respect to the substrate ATP. The second substrate of the reaction (the peptide) was kept at saturating concentrations (4-fold higher its K_m). Because (i) the ATP

dx.doi.org/10.1021/jm400233w | J. Med. Chem. 2013, 56, 5382−5394

concentration was limiting, i.e., [ATP] ≪ K_m(ATP), and (ii) the enzyme concentration was not negligible with respect to the ATP concentration, i.e., [E] ≥ [ATP], the classical Cheng−Prusoff relationship was not applicable. Consequently, K_i values were calculated according to eq 2: $K_i = (ID_{50} - E_0/2)/\{E_0 - [S_0/K_m - 1]/E_0\}$, where S_0 is the concentration of the competing substrate (ATP) and E_0 is the concentration of the enzyme. Each experiment was done in triplicate, and mean values were used for the interpolation. Curve fitting was performed with the program GraphPad Prism.

Enzymatic assay on isolated Abl. Recombinant human Abl was purchased from Upstate. Activity was measured in a filterbinding assay using an Abl specific peptide substrate (Abtide, Upstate). Reaction conditions were: 0.012 μM [γ-^{32}P]ATP, 50 μM peptide, 0.022 μM c-Abl. The apparent affinity (K_m) values of the Abl preparation used for its peptide, and ATP substrates were determined separately and found to be 1.5 μM and 10 μM, respectively. Kinetic analysis was performed as described for c-Src. Due to the noncompetitive mode of action and to the fact that the enzyme concentration was higher than the ATP substrate concentration, ID_{50} values were converted to K_i by eq 3: $K_i = ID_{50}/\{E_0 + [E_0(K_{m(ATP)}/S_0)]\}/E_0$, where E_0 and S_0 are the enzyme and the ATP concentrations, respectively. Each experiment was done in triplicate, and mean values were used for the interpolation. Curve fitting was performed with the program GraphPad Prism.

Cell Proliferation/Vitality Assay. In vitro experiments were carried out using the murine myeloblast-like cell lines 32D, 32D-p210, and 32D-T315I. These latter have been transfected with wild-type Bcr-Abl gene or the mutated form T315I, respectively. These cells have been kindly provided by Prof. M. A. Santucci (University of Bologna, Italy). Cells were cultured in RPMI medium with 10% FCS. Culture medium of parental cells 32D contained also 10 ng/mL IL-3. To determine antiproliferative effect of these pyrazolo[3,4-*d*]pyrimidines, 32D cells were seeded at 2 × 10^5 cells/mL density and treated with the compounds at increasing concentrations from 0.01 to 10 μM. The cultures were maintained at 37 °C in 5% v/v CO_2 for 48 or 72 h. Cell number and vitality were evaluated using the automatic cell counter NucleoCounter (Chemometec, Denmark). Results from the NucleoCounter represented either total or nonviable cell concentration, depending on the sample preparation indicated by manufacturer. IC_{50} (drug concentration that determined the 50% of growth inhibition) was calculated by Grafit 4 software using the best fitting sigmoid curve. For apoptosis evaluation, DNA was extracted from cells by incubating them for 1 h at 55 °C in 10% SDS and 20 mg/mL of proteinase K. After isolation with phenol/chloroform/isoamyl alcohol, the genomic DNA was loaded in 2% agarose gels containing ethidium bromide and the presence of fragmented DNA was visualized by UV transilluminator.

Apoptosis Assay on CD34+ from CML Patients. Bone marrow samples from Ph+ CML patients at diagnosis (n = 2) and Ph+ T315I mutant CML patients (n = 2) were collected after informed consent. Mononuclear cells were isolated by density gradient centrifugation in Ficoll-Hypaque and resuspended in RPMI medium with 10% FBS. Cells were seeded at 4 × 105 cells/mL density and treated with **2q**, **2j**, and DMSO vehicle control at increasing concentration from 1 to 20 μM for 48 h. After incubation time, cells were harvested and labeled for 15 min with antibodies against human CD34 and CD45 (APC Mouse Anti-Human CD34 and PerCP Mouse Anti-Human CD45, BD Pharmingen). To determine apoptotic effects of compounds, cells were washed with phosphate-buffered saline (PBS), resuspended in annexin buffer, and labeled for 15 min with Annexin V-FITC/propidium iodide (PI) (FITC Annexin V Apoptosis Detection Kit II, BD Pharmingen). At least 150000 events per samples were analyzed using a BD FACSCalibur flow cytometer. The expression levels were calculated as mean fluorescence intensity ratio of the antibodies divided by mean intensity of the controls.

Animals and Experimental in Vivo Model. Female CD1 nude mice (Charles River, Milan, Italy) were maintained under the guidelines established by host Institution (University of L'Aquila, Medical School and Science and Technology School Board Regulations, complying with the Italian government regulation no. 116, January 27, 1992, for the use of laboratory animals). Before any invasive manipulation, mice were anesthetized with a mixture of ketamine (25 mg/mL) and xylazine (5 mg/mL). Tumor grafts were obtained by injecting sc 1 ×106 32D cells in 100 μL of 12 mg/mL Matrigel (Becton Dickinson, Franklin Lakes, NJ, USA). Tumor growth was monitored daily by measuring the average tumor diameter. The tumor volume was expressed in mm^3 according to the formula $(width)^2 \times length/2$. For in vivo administration, **2j** was prepared as suspension in cremophor/ethanol/water solution (1:1:10, v/v/v). Each mouse received daily oral administration of cremophor vehicle or of 80 mg/kg **2j**. At the end point, tumor masses were excised from mice and processed for histological evaluation. Briefly, tissues were fixed in 4% formaldehyde in 0.1 M phosphate buffer, pH 7.2, and embedded in paraffin. Slide-mounted tissue sections (4 μm thick) were deparaffinized in xylene and hydrated serially in 100, 95, and 80% ethanol. Sections were washed three times in PBS and stained with hematoxylin and eosin stain method.

■ ASSOCIATED CONTENT

Supporting Information

Analytical data of compounds **2f−j** and **2l−z**, a table with elemental analysis for new synthesized compounds, and a table with binding free energies of to the Abl T315I mutant. This material is available free of charge via the Internet at http://pubs.acs.org.

■ AUTHOR INFORMATION

Corresponding Author

*For S.S.: phone, +39 010 3538866; fax, +39 010 3538358 E-mail, schensil@unige.it. For M.B.: phone, +39 0577 234306; fax, +39 0577 234306; E-mail, botta.maurizio@gmail.com.

Notes

The authors declare no competing financial interest.

■ ACKNOWLEDGMENTS

This work was partially supported by the Italian Association for Cancer Research AIRC IG_4538 grant to G.M., and by National Interest Research Projects (PRIN_2007_N7KYCY) to G.M., M.B., and S.S. (PRIN_2008_5HR5JK). Financial support has been also received from the Istituto Toscano Tumori-ITT-Grant proposal 2010. S.S. was also supported by the National Interest Research Project PRIN_2010_5YY2HL. The University of Siena is also acknowledged for financial support. We are grateful to Lead Discovery Siena Srl and Cost Action CM1106 "Chemical Approaches to Targeting Drug Resistance in Cancer Stem Cells". We thank Prof. Pietro Lupetti for liposomes morphological characterization. We are indebted to Molecular Discovery for access to the GRID code.

■ ABBREVIATIONS USED

Ph, Philadelphia chromosome; TK, tyrosine kinase; IM, imatinib; MM-GBSA, molecular mechanics/generalized born surface area; MIF, molecular interaction field; FEP, free energy perturbation; MC/FEP, Monte Carlo/free-energy perturbation; HLM, human liver microsomes; NPLA, number of planes of grid points per Angstrom; MSD, mass spectra detection; SUV, small unilamellar vesicle; TEM, transmission electron microscopy; FBS, fetal bovine serum; APC, antigen-presenting cell; FITC, fluorescein isothiocyanate; MR, membrane retention

■ REFERENCES

(1) Hantschel, O.; Superti-Furga, G. Regulation of the c-Abl and Bcr-Abl tyrosine kinases. *Nat. Rev. Mol. Cell Biol.* **2004**, *5*, 33−44.

(2) Deininger, M.; Buchdunger, E.; Druker, B. J. The development of imatinib as a therapeutic agent for chronic myeloid leukemia. *Blood* **2005**, *105*, 2640−2653.
(3) Jabbour, E.; Kantarjian, H. Chronic myeloid leukemia: 2012 update on diagnosis, monitoring, and management. *Am. J. Hematol.* **2012**, *87*, 1037−1045.
(4) Kantarjian, H.; Giles, F.; Wunderle, L.; Bhalla, K.; O'Brien, S.; Wassmann, B.; Tanaka, C.; Manley, P.; Rae, P.; Mietlowski, W.; Bochinski, K.; Hochhaus, A.; Griffin, J. D.; Hoelzer, D.; Albitar, M.; Dugan, M.; Cortes, J.; Alland, L.; Ottmann, O. G. Nilotinib in imatinib-resistant CML and Philadelphia chromosome-positive ALL. *N. Engl. J. Med.* **2006**, *354*, 2542−2551.
(5) Shah, N. P.; Tran, C.; Lee, F. Y.; Chen, P.; Norris, D.; Sawyers, C. L. Overriding imatinib resistance with a novel ABL kinase inhibitor. *Science* **2004**, *305*, 399−401.
(6) O'Hare, T.; Eide, C. A.; Deininger, M. W. New Bcr-Abl inhibitors in chronic myeloid leukemia: keeping resistance in check. *Expert Opin. Invest. Drugs* **2008**, *17*, 865−878.
(7) Schenone, S.; Brullo, C.; Botta, M. New opportunities to treat the T315I-Bcr-Abl mutant in chronic myeloid leukaemia: tyrosine kinase inhibitors and molecules that act by alternative mechanisms. *Curr. Med. Chem.* **2010**, *17*, 1220−1245.
(8) Golas, J. M.; Arndt, K.; Etienne, C.; Lucas, J.; Nardin, D.; Gibbons, J.; Frost, P.; Ye, F.; Boschelli, D. H.; Boschelli, F. SKI-606, a 4-anilino-3-quinolinecarbonitrile dual inhibitor of Src and Abl kinases, is a potent antiproliferative agent against chronic myelogenous leukemia cells in culture and causes regression of K562 xenografts in nude mice. *Cancer Res.* **2003**, *63*, 375−381.
(9) Kimura, S.; Naito, H.; Segawa, H.; Kuroda, J.; Yuasa, T.; Sato, K.; Yokota, A.; Kamitsuji, Y.; Kawata, E.; Ashihara, E.; Nakaya, Y.; Naruoka, H.; Wakayama, T.; Nasu, K.; Asaki, T.; Niwa, T.; Hirabayashi, K.; Maekawa, T. NS-187, a potent and selective dual Bcr-Abl/Lyn tyrosine kinase inhibitor, is a novel agent for imatinib-resistant leukemia. *Blood* **2005**, *106*, 3948−3954.
(10) O'Hare, T.; Pollock, R.; Stoffregen, E. P.; Keats, J. A.; Abdullah, O. M.; Moseson, E. M.; Rivera, V. M.; Tang, H.; Metcalf, C. A., III; Bohacek, R. S.; Wang, Y.; Sundaramoorthi, R.; Shakespeare, W. C.; Dalgarno, D.; Clackson, T.; Sawyer, T. K.; Michael, W.; Deininger, M. W.; Druker, B. J. Inhibition of wild-type and mutant Bcr-Abl by AP23464, a potent ATP-based oncogenic protein kinase inhibitor: implications for CML. *Blood* **2004**, *104*, 2532−2539.
(11) Huron, D. R.; Gorre, M. E.; Kraker, A. J.; Sawyers, C. L.; Rosen, N.; Moasser, M. M. A novel pyridopyrimidine inhibitor of abl kinase is a picomolar inhibitor of Bcr-abl-driven K562 cells and is effective against STI571-resistant Bcr-Abl mutants. *Clin. Cancer Res.* **2003**, *9*, 1267−1273.
(12) Huang, W. S.; Metcalf, C. A.; Sundaramoorthi, R.; Wang, Y.; Zou, D.; Thomas, R. M.; Zhu, X.; Cai, L.; Wen, D.; Liu, S.; Romero, J.; Qi, J.; Chen, I.; Banda, G.; Lentini, S. P.; Das, S.; Xu, Q.; Keats, J.; Wang, F.; Wardwell, S.; Ning, Y.; Snodgrass, J. T.; Broudy, M. I.; Russian, K.; Zhou, T.; Commodore, L.; Narasimhan, N. I.; Mohemmad, Q. K.; Iuliucci, J.; Rivera, V. M.; Dalgarno, D. C.; Sawyer, T. K.; Clackson, T.; Shakespeare, W. C. Discovery of 3-[2-(imidazo[1,2-*b*]pyridazin-3-yl)ethynyl]-4-methyl-*N*-{4-[(4-methylpiperazin-1-yl)methyl]-3-(trifluoromethyl)phenyl}benzamide (AP24534), a potent, orally active pan-inhibitor of breakpoint cluster region-abelson (BCR-ABL) kinase including the T315I gatekeeper mutant. *J. Med. Chem.* **2010**, *53*, 4701−4719.
(13) Gozgit, J. M.; Wong, M. J.; Moran, L.; Wardwell, S.; Mohemmad, Q. K.; Narasimhan, N. I.; Shakespeare, W. C.; Wang, F.; Clackson, T.; Rivera, V. M. Ponatinib (AP24534), a multitargeted pan-FGFR inhibitor with activity in multiple FGFR-amplified or mutated cancer models. *Mol. Cancer Ther.* **2012**, *11*, 690−699.
(14) Azam, M.; Latek, R. R.; Daley, G. Q. Mechanisms of autoinhibition and STI-571/imatinib resistance revealed by mutagenesis of BCR-ABL. *Cell* **2003**, *112*, 831−843.
(15) Martinelli, G.; Soverini, S.; Rosti, G.; Baccarani, M. Dual tyrosine kinase inhibitors in chronic myeloid leukemia. *Leukemia* **2005**, *19*, 1872−1879.
(16) Apsel, B.; Blair, J. A.; Gonzalez, B.; Nazif, T. M.; Feldman, M. E.; Aizenstein, B.; Hoffman, R.; Williams, R. L.; Shokat, K. M.; Knight, Z. A. Targeted polypharmacology: discovery of dual inhibitors of tyrosine and phosphoinositide kinases. *Nature Chem. Biol.* **2008**, *4*, 691−699.
(17) (a) Schenone, S.; Botta, M.; Radi, M.; Bruno, O. New insights into small-molecule inhibitors of Bcr-Abl. *Med. Res. Rev.* **2011**, *31*, 1−41. (b) Schenone, S.; Bruno, O.; Radi, M.; Botta, M. 4-Amino-substituted pyrazolo[3,4-*d*]pyrimidines: synthesis and biological properties. *Mini-Rev. Org. Chem.* **2009**, *6*, 220−233.
(18) Radi, M.; Brullo, C.; Crespan, E.; Tintori, C.; Musumeci, F.; Biava, M.; Schenone, S.; Dreassi, E.; Zamperini, C.; Maga, G.; Pagano, D.; Angelucci, A.; Bologna, M.; Botta, M. Identification of potent c-Src inhibitors strongly affecting the proliferation of human neuroblastoma cells. *Bioorg. Med. Chem. Lett.* **2011**, *21*, 5928−5933.
(19) Radi, M.; Dreassi, E.; Brullo, C.; Crespan, E.; Tintori, C.; Bernardo, V.; Valoti, M.; Zamperini, C.; Daigl, H.; Musumeci, F.; Carraro, F.; Naldini, A.; Filippi, I.; Maga, G.; Schenone, S.; Botta, M. Design, synthesis, biological activity, and ADME properties of pyrazolo[3,4-*d*]pyrimidines active in hypoxic human leukemia cells: a lead optimization study. *J. Med. Chem.* **2011**, *54*, 2610−2626.
(20) Santucci, M. A.; Corradi, V.; Mancini, M.; Manetti, F.; Radi, M.; Schenone, S.; Botta, M. C6-Unsubstituted pyrazolo[3,4-*d*]pyrimidines are dual Src/Abl inhibitors effective against imatinib mesylate resistant chronic myeloid leukemia cell lines. *ChemMedChem* **2009**, *4*, 118−126.
(21) Carraro, F.; Naldini, A.; Pucci, A.; Locatelli, G. A.; Maga, G.; Schenone, S.; Bruno, O.; Ranise, A.; Bondavalli, F.; Brullo, C.; Fossa, P.; Menozzi, G.; Mosti, L.; Modugno, M.; Tintori, C.; Manetti, F.; Botta, M. Pyrazolo[3,4-*d*]pyrimidines as potent antiproliferative and proapoptotic agents toward A431 and 8701-BC cells in culture via inhibition of c-Src phosphorylation. *J. Med. Chem.* **2006**, *49*, 1549−1561.
(22) Santucci, M. A.; Mancini, M.; Corradi, V.; Iacobucci, I.; Martinelli, G.; Botta, M.; Schenone, S. New SRC/ABL inhibitors for chronic myeloid leukemia therapy show selectivity for T315I ABL mutant $CD34^+$ cells. *Invest. New Drugs* **2010**, *28*, 876−878.
(23) Zhou, T.; Parillon, L.; Li, F.; Wang, Y.; Keats, J.; Lamore, S.; Xu, Q.; Shakespeare, W.; Dalgarno, D.; Zhu, X. Crystal structure of the T315I mutant of AbI kinase. *Chem. Biol. Drug. Des.* **2007**, *70*, 171−181.
(24) Bounaud, P. Y.; Gosberg, A.; Hendle, J.; Lewis, H. A.; Romero, R.; Wilson, M. E.; Zhang, F. Crystal structure of mutant ABL kinase domain in complex with small molecule fragment. *Protein Data Bank* 2009, DOI:10.2210/pdb3dk7/pdb.
(25) Modugno, M.; Casale, E.; Soncini, C.; Rosettani, P.; Colombo, R.; Lupi, R.; Rusconi, L.; Fancelli, D.; Carpinelli, P.; Cameron, A. D.; Isacchi, A.; Moll, J. Crystal structure of the T315I Abl mutant in complex with the aurora kinases inhibitor PHA-739358. *Cancer Res.* **2007**, *67*, 7987−7990.
(26) O'Hare, T.; Shakespeare, W. C.; Zhu, X.; Eide, C. A.; Rivera, V. M.; Wang, F.; Adrian, L. T.; Zhou, T.; Huang, W. S.; Xu, Q.; Metcalf, C. A., III; Tyner, J. W.; Loriaux, M. M.; Corbin, A. S.; Wardwell, S.; Ning, Y.; Keats, J. A.; Wang, Y.; Sundaramoorthi, R.; Thomas, M.; Zhou, D.; Snodgrass, J.; Commodore, L.; Sawyer, T. K.; Dalgarno, D. C.; Deininger, M. W.; Druker, B. J.; Clackson, T. AP24534, a pan-BCR-ABL inhibitor for chronic myeloid leukemia, potently inhibits the T315I mutant and overcomes mutation-based resistance. *Cancer Cell.* **2009**, *16*, 401−412.
(27) Zhou, T.; Commodore, L.; Huang, W. S.; Wang, Y.; Thomas, M.; Keats, J.; Xu, Q.; Rivera, V. M.; Shakespeare, W. C.; Clackson, T.; Dalgarno, D. C.; Zhu, X. Structural mechanism of the Pan-BCR-ABL inhibitor ponatinib (AP24534): lessons for overcoming kinase inhibitor resistance. *Chem. Biol. Drug. Des.* **2011**, *77*, 1−11.
(28) Chan, W. W.; Wise, S. C.; Kaufman, M. D.; Ahn, Y. M.; Ensinger, C. L.; Haack, T.; Hood, M. M.; Jones, J.; Lord, J. W.; Lu, W. P.; Miller, D.; Patt, W. C.; Smith, B. D.; Petillo, P. A.; Rutkoski, T. J.; Telikepalli, H.; Vogeti, L.; Yao, T.; Chun, L.; Clark, R.; Evangelista, P.; Gavrilescu, L. C.; Lazarides, K.; Zaleskas, V. M.; Stewart, L. J.; Van Etten, R. A.; Flynn, D. L. Conformational control inhibition of the BCR-ABL1 tyrosine kinase, including the gatekeeper T315I mutant, by

the switch-control inhibitor DCC-2036. *Cancer Cell* **2011**, *19*, 556−568.
(29) Manetti, F.; Pucci, A.; Magnani, M.; Locatelli, G. A.; Brullo, C.; Naldini, A.; Schenone, S.; Maga, G.; Carraro, F.; Botta, M. Inhibition of Bcr-Abl phosphorylation and induction of apoptosis by pyrazolo-[3,4-*d*]pyrimidines in human leukemia cells. *ChemMedChem* **2007**, *2*, 343−353.
(30) *Grid 22*; Molecular Discovery Ltd: Pinner, Middlesex, U.K., 2004.
(31) Jorgensen, W. L.; Schyman, P. Treatment of halogen bonding in the OPLS-AA force field: application to potent anti-HIV agents. *J. Chem. Theory Comput.* **2012**, *8*, 3895−3901.
(32) Dreassi, E.; Zizzari, A. T.; Mori, M.; Filippi, I.; Belfiore, A.; Naldini, A.; Carraro, F.; Santucci, A.; Schenone, S.; Botta, M. 2-Hydroxypropyl-*β*-cyclodextrin strongly improves water solubility and anti-proliferative activity of pyrazolo[3,4-*d*]pyrimidines Src-Abl dual inhibitors. *Eur. J. Med. Chem.* **2010**, *45*, 5958−5964.
(33) (a) Avdeef, A. High-throughput measurements of solubility profiles. Pharmacokinetic optimization in drug research: biological, physicochemical, and computational strategies. LogP2000, 2nd Lipophilicity Symposium, Lausanne, Switzerland, March 5−9, 2000, pp 305−325. (b) Bard, B.; Martel, S.; Carrupt, P. A. High throughput UV method for the estimation of thermodynamic solubility and the determination of the solubility in biorelevant media. *Eur. J. Pharm. Sci.* **2008**, *33*, 230−240.
(34) Verdonk, M. L.; Cole, J. C.; Hartshorn, M. J.; Murray, C. W.; Taylor, R. D. Improved protein−ligand docking using GOLD. *Proteins* **2003**, *52*, 609−623.
(35) *Maestro*, version 9.1; Schrödinger, LLC: Portland, OR, 2007; www.schrodinger.com.
(36) Jorgensen, W. L.; Thomas, L. T. Perspective on free-energy perturbation calculations for chemical equilibria. *J. Chem. Theory Comput.* **2008**, *4*, 869−876.
(37) Jorgensen, W. L.; Tirado-Rives, J. Molecular modeling of organic and biomolecular systems using BOSS and MCPRO. *J. Comput. Chem.* **2005**, *26*, 1689−1700.
(38) Zeevaart, J. G.; Wang, L.; Thakur, V. V.; Leung, C. S.; Tirado-Rives, J.; Bailey, C. M.; Domaoal, R. A.; Anderson, K. S.; Jorgensen, W. L. Optimization of azoles as anti-HIV agents guided by free-energy calculations. *J. Am. Chem. Soc.* **2008**, *130*, 9492−9499.
(39) Leung, C. S.; Zeevaart, J. G.; Domaoal, R. A.; Bollini, M.; Thakur, V. V.; Spasov, K.; Anderson, K. S.; Jorgensen, W. L. Eastern extension of azoles as non-nucleoside inhibitors of HIV-1 reverse transcriptase; cyano group alternatives. *Bioorg. Med. Chem. Lett.* **2010**, *20*, 2485−2488.
(40) Jorgensen, W. L.; Tirado-Rives, J. Potential energy functions for atomic-level simulations of water, and organic and biomolecular systems. *Proc. Natl. Acad. Sci. U. S. A.* **2005**, *102*, 6665−6670.
(41) (a) Manetti, F.; Brullo, C.; Magnani, M.; Mosci, F.; Chelli, B.; Crespan, E.; Schenone, S.; Naldini, A.; Bruno, O.; Trincavelli, M. L.; Maga, G.; Carraro, F.; Martini, C.; Bondavalli, F.; Botta, M. Structure-based optimization of pyrazolo[3,4-*d*]pyrimidines as Abl inhibitors and antiproliferative agents toward human leukemia cell lines. *J. Med. Chem.* **2008**, *51*, 1252−1259. (b) Falchi, F.; Manetti, F.; Carraro, F.; Naldini, A.; Maga, G.; Crespan, E.; Schenone, S.; Bruno, O.; Brullo, C.; Botta, M. 3D QSAR models built on structure-based alignments of Abl tyrosine kinase inhibitors. *ChemMedChem* **2009**, *4*, 976−987. (c) Crespan, E.; Radi, M.; Zanoli, S.; Schenone, S.; Botta, M.; Maga, G. Dual Src and Abl inhibitors target wild type Abl and the Abl T315I Imatinib-resistant mutant with different mechanisms. *Bioorg. Med. Chem.* **2010**, *18*, 3999−4008.
(42) Brik, A.; Wu, C.; Best, M. D.; Wong, C. Tetrabutylammonium fluoride-assisted rapid *N*9-alkylation on purine ring: application to combinatorial reactions in microtiter plates for the discovery of potent sulfotransferase inhibitors in situ. *Bioorg. Med. Chem.* **2005**, *13*, 4622−4626.
(43) Wohnsland, F.; Faller, B. High-throughput permeability pH profile and high-throughput alkane/water log *P* with artificial membranes. *J. Med. Chem.* **2001**, *44*, 923−930.